Simple Model for Base Pressure Effects in Source Flow Chemical Lasers

Kerry E. Patterson,* Jad H. Batteh,† and Steade S. Howie‡
Science Applications, Inc., Marietta, Georgia

A simple model is developed to investigate the effects of base pressure on the performance of source flow chemical lasers. The laser flowfield is divided into two coupled, one-dimensional regions representing the pure source flow region and a region influenced by the base pressure. The differential equations describing the gasdynamics, mixing, reaction, and lasing in the two regions are formulated. The model indicates that lasing performance decreases as the base pressure increases. However, performance can approach and even exceed that of a pure source flow laser if the base pressure is controlled.

I. Introduction

CONSIDERABLE effort currently is being expended to develop high-power, high-efficiency source flow chemical lasers. Figure 1 shows a typical source flow laser configuration. These lasers are characterized by supersonic oxidizer streams which enter the laser cavity from an array of source flow nozzles. A secondary fuel stream is injected either sonically or supersonically into the oxidizer stream through holes in wedges placed at the exit of the source flow nozzle. The mixing of the two streams and the subsequent reaction generates vibrationally excited molecules that are the source of the laser radiation. As indicated by the figure, the plane in which mixing occurs is orthogonal to the expansion plane and the lasing axis. The purpose of the source flow is to reduce the amount of diluent required by using area expansion to help control the temperature and pressure rise in the laser cavity.

In Ref. 1 we developed a simple model for analyzing a continuous wave, source flow HF chemical laser. In that model the effect of the base region between nozzles on the gasdynamics in the laser cavity was ignored and the flowfield was modeled, in an average sense, as a pure source flow. The purpose of this analysis is to extend the theory of Ref. 1 to include the effects of the base region on the cavity gasdynamics and kinetics, and to investigate how the pressure in the base affects lasing performance. As in Ref. 1, we focus on the HF laser pumped by the reaction of F and H_2 but the basic theory can be applied to a number of chemical laser concepts.

The flowfield in the laser cavity represents a complex, three-dimensional, chemically reacting flow. Aside from the obvious numerical difficulties associated with characterizing this flow in detail, additional problems arise because many of the physical processes occurring in the cavity are not well understood. For example, the pressure of the fuel stream as it exits the wedges is generally one or two orders of magnitude greater than that of the oxidizer stream flowing over the wedges. The process of pressure equilibration for the two steams and their subsequent mixing and reaction have yet to be analyzed in detail. In addition, techniques for determining the value of the pressure in the base region between nozzles and its effect on the flowfield are far from standardized, even though this problem has been the subject of extensive research because of it application to base drag reduction in projectiles.[2] Consequently, in our analysis a number of approximations must be introduced to make the problem tractable. The justification of these approximations and their effect on the solution will be discussed in the following sections.

Received Dec. 3, 1981; presented as Paper 82-0399 at the AIAA 20th Aerospace Sciences Meeting, Orlando, Fla., Jan. 11-14, 1982; revision received Dec. 7, 1982.

*Senior Staff Scientist. Member AIAA.
†Staff Scientist.
‡Division Manager; currently Deputy Operations Manager, Electromagnetics Technology Operation, SAI, McLean, Va.

II. Theory

Figure 2 shows a schematic representation of the flowfield in the expansion plane of a source flow chemical laser. The flowfield shown in the figure represents a radially expanding, chemically reacting plume which may be either over- or underexpanded depending on whether the base pressure p_b is less than or greater than the nozzle exit pressure. In our analysis we divide the cavity flowfield into two regions—a source flow region (denoted by A in the figure), which is the region of flow that has not yet been influenced by the base pressure, and a base pressure flow region (denoted by B), which consists of that portion of the original source flow that has been altered by the base pressure. These two regions are assumed to be separated by an entrainment boundary depicted by the dashed line originating at S′ in Fig. 2.

In the following sections, we will develop the equations necessary to describe the gasdynamics, mixing and reaction kinetics, and lasing characteristics of these two flow regions.

A. Gasdynamic Analysis

As in Ref. 1, we first derive equations for the "average" gasdynamic properties in the laser cavity, based on the assumption that the flow variables are independent of y, the co-ordinate transverse to the expansion plane shown in Fig. 2. The flow properties at the nozzle exit, denoted by the radius r_i, are the initial conditions for the calculation. These conditions are obtained by instantaneously mixing the fuel and oxidizer streams, without allowing them to react, and bringing them to a common pressure.

The A-region gasdynamic equations are essentially the same as those derived in Ref. 1 for a pure source flow. They depend only on the radial coordinate r, and for constant specific heats, they reduce to a single differential equation for the Mach number

$$\frac{dM_a^2}{dr} = \frac{M_a^2}{1-M_a^2}\left(1+\frac{\gamma-1}{2}M_a^2\right)\left[\frac{-2}{r}+\frac{1+\gamma M_a^2}{T_{0_a}}\frac{dT_{0_a}}{dr}\right] \quad (1)$$

and algebraic relations for the remaining gasdynamic parameters.[3] In Eq. (1), we have introduced the subscript a to denote properties in the A region. Thus, M_a and T_{0_a} represent the Mach number and total temperature in the A region, respectively. The ratio of specific heats γ is constant and taken to be the same for both regions. An expression for the change in total temperature will be derived in Sec. II.C. when we discuss the lasing equations.

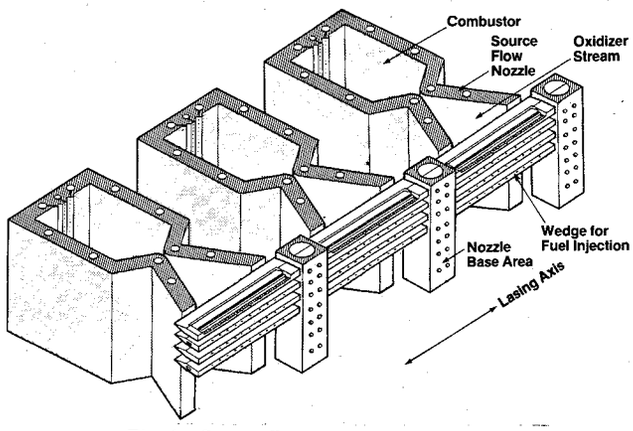

Fig. 1 Source flow chemical laser concept.

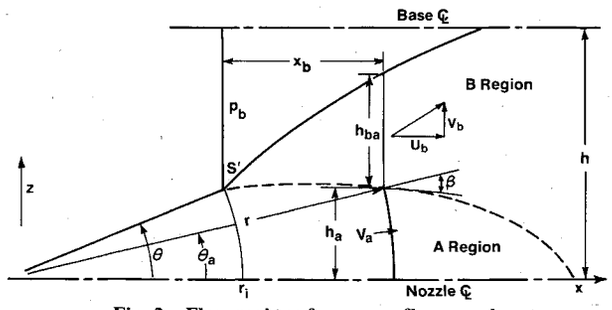

Fig. 2 Flow regions for source flow nozzle.

The gasdynamic properties of the B region are more complex than those of the source flow region. In writing the conservation equations for this region, it is necessary to account for the entrainment of mass, momentum, and energy from the source flow into the base region. In addition, the flow characteristics in the base vary considerably, ranging from supersonic, approximately inviscid flow near the entrainment boundary, to highly viscous, subsonic flow in the recirculation region of the base. In our analysis we will treat explicitly only the supersonic, inviscid portion of the base flow, which we assume to extend to a height h_{ba} above the entrainment boundary. The effect of the recirculation region on both the lasing and cavity gasdynamics is treated in the following approximate manner. We assume, first, that sufficient purge is introduced into the base to remove the ground-state species, but that this purge flow is sufficiently low that it does not significantly influence the supersonic base flow. Thus, we assume that the recirculation zone has zero gain, and we neglect the effect of the purge flow on the cavity gasdynamics. The other dominant influence of the viscous base flow is that in the absence of external influences the viscous interaction of the wakes from adjacent plumes establishes the value of the base pressure. For this analysis, we assume that the base pressure is obtained either from experiment or from semi-empirical correlations such as those discussed in Ref. 4.

To further simplify the calculation, we calculate only average properties for the B region by assuming that the gasdynamic properties are a function only of x. The conservation equations for the B region can be readily derived from a control volume analysis based on the geometry of Fig. 2.[4] All of the flow entrained into the base is assumed to be contained within the outer boundary specified by h_{ba}. In Fig. 2, x_b denotes the x location of the entrainment boundary measured from S′, and is defined by the geometric relationship

$$\frac{dx_b}{dr} = G = \cos\theta_a + \sin\theta_a \tan\beta \tag{2}$$

Assuming that at any axial station x_b, the flow properties in the B-region are uniform, leads to the following equations for the conservation of mass, x momentum, z momentum, and energy:

$$\frac{d\dot{m}_b}{dr} = E\dot{m}_b \tag{3}$$

$$\frac{du_b}{dr} = E(V_a\cos\theta_a - u_b) + (p_b - p_a)(\sin\theta_a - \cos\theta_a\tan\beta)/\dot{m}_b - \frac{h_{ba}}{\dot{m}_b}\frac{dp_b}{dr} \tag{4}$$

$$\frac{dv_b}{dr} = E(V_a\sin\theta_a - v_b) + (p_a - p_b)\frac{G}{\dot{m}_b} \tag{5}$$

$$\frac{dT_{0_b}}{dr} = E(T_{0_a} - T_{0_b}) + \left(\frac{dT_{0_b}}{dr}\right)_R \tag{6}$$

In these equations, $\dot{m}_b$ is the flow rate in the B region per unit height in the y direction

$$\dot{m}_b = \rho_b u_b h_{ba} \tag{7}$$

where ρ_b and u_b are the density and the x velocity, respectively, in the B region. (In general, we will use the subscript b to denote properties in the B region). V_a is the radial velocity in the source flow at radius r, p_a the source flow pressure, v_b the z component of the velocity in the B region, and T_{0_b} the total temperature in the B region. The entrainment coefficient E is given by

$$E = \dot{m}\tan\beta/\dot{m}_b r\theta \tag{8}$$

where θ is the source flow half-angle at the nozzle exit and

$$\dot{m} = \rho_i V_i r_i \theta \tag{9}$$

is the total mass flow rate in the cavity shown in Fig. 2 per unit height in the y direction. The terms containing E on the right-hand sides of Eqs. (3-6) represent the effect of entrainment from the source flow. The last term in Eq. (6), which represents the increase in total temperature in the B region due to chemical reactions, will be evaluated in Sec. II.C. In writing Eq. (6), we have assumed that the specific heats in the A and B regions are equal and independent of r.

The angle θ_a is defined by the geometric relationship

$$\frac{d\theta_a}{dr} = -\frac{\tan\beta}{r} \tag{10}$$

For the case where the base pressure is less than the source flow pressure, we take β to be the Mach angle for the leading expansion wave, i.e.,

$$\beta = \sin^{-1}(1/M_a) \tag{11}$$

If $p_b > p_a$, then β is the shock inclination angle, which can be approximated by

$$\beta = \sin^{-1}\left[\frac{(\gamma+1)p_b/p_a + \gamma - 1}{2\gamma M_a^2}\right]^{1/2} \tag{12}$$

for weak shock waves.[5]

In solving the equations for the B region, we assume that the pressure remains constant at the value p_b until all the available base area is filled, i.e., until the outer edge of the plume strikes the base centerline. Measurements in

nonreacting, supersonic base flows indicate that the pressure in the base region remains nearly constant until the edge of the supersonic flow approaches the centerline.[6] At that point, the pressure increases as the flow is turned parallel to the centerline. Although these measurements lend some credence to the constant pressure assumption, they do not fully justify it, since, in our case, reactions and heat release are occurring in the base region as well as in the source flow. Although we do not permit the base pressure to vary with x in response to these processses, we do account for the heat release in the correlation which establishes the value of p_b, as discussed in Ref. 4.

Our analysis is not continued beyond the impingement point because, in practice, chemical laser nozzles are generally designed so that lasing terminates before impingement to avoid the deleterious pressure rise. Consequently, for this analysis we take p_b to be constant and neglect the term containing dp_b/dr in Eq. (4).

To close the system of equations, we need the equation of state for the B region

$$p_b = \rho_b R_u T_b / \bar{M} \tag{13}$$

where R_u is the universal gas constant and $\bar{M}$ is the average molecular weight of the mixture. With the base pressure specified, we now have enough equations to determine the gasdynamic properties of the B region (ρ_b, T_b, u_b, v_b) and its geometric properties (θ_a, h_{ba}).

B. Mixed Zone Analysis

Although the fuel and oxidizer streams are assumed to be premixed in calculating the average gasdynamic properties, we include the effects of finite mixing by limiting the region where chemical reactions and lasing occur to a mixed zone between the wedges. This mixed zone is assumed to extend from the wedge centerline to the flame sheet boundary defined by

$$y' = y_f / w = [(r - r_i)/l_m]^m \tag{14}$$

where w is half the distance between wedges, l_m the mixing length, and m either 1 or ½ for turbulent or laminar mixing, respectively. For $r - r_i > l_m$, y' is, of course, equal to unity. The mixed zones in both the A and B regions are assumed to grow at the same rate, but the gasdynamic properties of the two mixed zones, in general, will be different.

In analyzing a specific laser design, we generally take $m = ½$ and calculate l_m based on the growth rate for laminar, incompressible, nonreacting shear layers. A factor of order unity is then applied to the calculated mixing rate in order to obtain better agreement with experimental data. Although the factor is allowed to change whenever the nozzle/wedge design changes, it is kept fixed when analyzing the effect of throughput or composition variation for a given design.

Chemical reactions and lasing are assumed to occur at the thermodynamic conditions and species concentrations characteristic of the mixed zones, and all reaction products are confined to the mixed zone. We will use the procedure developed in Ref. 1 for relating the mixed zone properties to the average gasdynamic properties. In accordance with that analysis, the mixed zone thermodynamic properties are related to the average gasdynamic properties by

$$p_m = p \tag{15}$$

$$T_m = T_{m_i}(1 - y') + y' T \tag{16}$$

$$\rho_m = \bar{M} p / R_u T_m \tag{17}$$

In Eq. (16) T_{m_i} is the wedge wall temperature which is introduced to account for the fact that the oxidizer flow initially entrained into the mixed zone originates in the wedge boundary layer. Equations (15-17) are applied to both the A and B region mixed zones by using the appropriate average gasdynamic properties on the right-hand sides of the equations. T_{m_i} is taken to be the same for both regions.

For all species except F, H_2, HF, and H the mixed zone mass fractions are given by

$$C_{s_m} = C_{s_i} \tag{18}$$

where C_{s_i} is the mass fraction of species S at the exit. The remaining species are coupled through the pumping reaction

$$F + H_2 \rightarrow HF + H \tag{19}$$

with the result that

$$C_{s_m} = C_{s_i} - \frac{M_s}{y' M_{HF}} C_{HF} \tag{20}$$

for $S = F$ and H_2, and

$$C_{H_m} = \frac{M_H}{y' M_{HF}} C_{HF} \tag{21}$$

In Eqs. (20) and (21), M_s represents the molecular weight of species S and C_{HF} is the flow average mass fraction of HF, which is related to the mixed zone mass fraction by

$$C_{HF} = y' C_{HF_m} \tag{22}$$

Equations (20) and (21) are used for both regions by using the appropriate value of C_{HF}.

It is convenient to express the global concentrations of HF in the A and B regions in terms of pumping parameters

$$X_{T_a} = M_F C_{HF_a} / M_{HF} C_{F_i}, \quad X_{T_b} = M_F C_{HF_b} / M_{HF} C_{F_i} \tag{23}$$

These parameters represent the ratio of the number of moles of HF in the two regions to the total number which would be created if all the fluorine were reacted. Then, for the most common case where the mixed stream is fuel rich, X_{T_a} and X_{T_b} would both be less than unity and would approach unity as the pumping reaction goes to completion. In terms of X_{T_a}, the pumping equation for HF in the source flow region is given by

$$\frac{dX_{T_a}}{dr} = \frac{\theta M_F}{\dot{m} M_{HF} C_{F_i}} r \dot{\omega}_{HF_a} \tag{24}$$

where the production rate of HF is given by

$$\dot{\omega}_{HF_a} = y' \left[\frac{\rho_m^2 C_{F_m} C_{H_{2m}} M_{HF}}{M_F M_{H_2}} k_p(T_m) \right]_A \tag{25}$$

In Eq. (25), k_p is the reaction rate in cm³/mole-s for the pumping reaction, Eq. (19), and the subscript to the bracket indicates that the mixed zone properties of the A region are to be used.

For the B region

$$\frac{dX_{T_b}}{dr} = E(X_{T_a} - X_{T_b}) + \frac{M_F}{M_{HF} C_{F_i}} \frac{G h_{ba} \dot{\omega}_{HF_b}}{\dot{m}_b} \tag{26}$$

where E is the entrainment coefficient, G the geometric parameter defined by Eq. (2), and $\dot{\omega}_{HF_b}$ is calculated using the mixed zone properties of the B region.

C. Lasing Analysis

In Ref. 1 we developed a method for estimating the chemical efficiency of a source flow laser which lases simultaneously on several vibrational transitions. That analysis was based on the work of Mirels,[7] Broadwell,[8] and Emanuel and Whittier,[9] extended to account for streamwise variations in the gasdynamic parameters and for multiquantum deactivation processes. That formulation will be modified here to account for the presence of the B region.

The lasing model is based on the following assumptions. The rotational levels of each vibrational level of HF are assumed to be in rotational equilibrium at the translational temperature of the mixed zone so that only one rotational-vibrational line is assumed to lase in each vibrational manifold. Only P branch transitions, corresponding to the lasing transition $(v+1,\ J-1)\rightarrow(v,J)$, are considered and the value for J is taken to be the same for each transition. The value of the gain for each lasing transition is taken to be the same, although the common value of the gain depends on the region of the flowfield, A or B, as well as the parameter r. The total laser output is then calculated for a Fabry-Perot optical cavity using the gain equals loss approximation.

A convenient measure of lasing efficiency is the chemical specific efficiency η, defined by

$$\eta = P/\dot{m}C_{\mathrm{F}_i}w \tag{27}$$

where P is the total laser power from the single mixing segment bounded by the wedge centerline and the centerline between wedges and η represents the lasing energy extracted per gram of fluorine flowing through the cavity. The chemical efficiency for the optical cavity can be estimated from the equation

$$\frac{\mathrm{d}\eta}{\mathrm{d}r} = \left(\frac{\mathrm{d}\eta}{\mathrm{d}r}\right)_A + \left(\frac{\mathrm{d}\eta}{\mathrm{d}r}\right)_B \tag{28}$$

where

$$\left(\frac{\mathrm{d}\eta}{\mathrm{d}r}\right)_A = \frac{y'h_a}{\dot{m}C_{\mathrm{F}_i}} g_{m_a} \sum_{v=0}^{v_f-1} I_v \tag{29}$$

and

$$\left(\frac{\mathrm{d}\eta}{\mathrm{d}r}\right)_B = \frac{y'h_{ba}G}{\dot{m}C_{\mathrm{F}_i}} g_{m_b} \sum_{v=0}^{v_f-1} I_v \tag{30}$$

represent the contributions to the chemical efficiency from the A and B regions, respectively. In Eqs. (29) and (30), I_v is the lasing intensity for the $v+1\rightarrow v$ transition, g_{m_a} and g_{m_b} are the gains in the mixed zones of the A and B regions, respectively, and v_f denotes the highest vibrational level which participates in a lasing transition. Equations (29) and (30), as written, reflect our assumption that lasing is confined to the mixed zone of the nozzle. We have also assumed that the gain is sufficiently low, so that each nozzle in the array experiences essentially the same intensity field. As discussed in Ref. 1, Eq. (29) is based on a source-flow description for the A region even though the intensity field is actually a function of x_b and not r. Nonetheless, Eq. (29) should provide a reasonable estimate for the lasing efficiency in the source flow region for moderate source flow angles.

For lasing to occur, the combined gain in the A and B regions must satisfy the threshold gain relationship

$$g_{m_a}h_a + g_{m_b}h_{ba} = hg_{\mathrm{th}}/y' \tag{31}$$

If the optical cavity is bounded by mirrors with reflectivities R_1 and R_2,

$$g_{\mathrm{th}} = -\ell n(R_1R_2)/4N_nh \tag{32}$$

where N_n denotes the number of primary nozzles in the array. In writing Eq. (31), we have used the threshold gain condition appropriate for the case where the wedges in adjacent nozzles are offset or canted.[1]

Expressions for the right-hand sides of Eqs. (29) and (30) can be obtained in a manner analogous to that used in Ref. 1 for the pure source flow case. The contribution to η from the B region can be written in the form

$$\left(\frac{\mathrm{d}\eta}{\mathrm{d}r}\right)_B = \frac{\dot{m}_b}{\dot{m}}\left\{\frac{\mathrm{d}}{\mathrm{d}r}(\eta_{\max_b}X_{T_b} - S_{l_b}) - D_bX_{T_b} - S_{2_b} + E\left[\eta_{\max_b}X_{T_b} - S_{l_b} - \frac{\theta}{\sin\theta}(\eta_{\max_a}X_{T_a} - S_{l_a})\right]\right\} \tag{33}$$

where

$$\eta_{\max_b} = \frac{\epsilon}{M_{\mathrm{F}}} \sum_{v=0}^{v_f} v[a_p(v) - F_v(T_{m_b})] \tag{34}$$

$$S_{l_b} = \frac{\epsilon g_{m_b}y'}{C_{\mathrm{F}_i}\rho_{m_b}\sigma_{0_b}} \sum_{v=0}^{v_f} vH_v(T_{m_b}) \tag{35}$$

$$D_b = \frac{\epsilon h_{ba}\rho_{m_b}^2 G}{\dot{m}_bM_{\mathrm{F}}} \sum_S \frac{C_{S_{mb}}}{M_S} \sum_{v=0}^{v_f} F_v(T_{m_b})k_{S_v}(T_{m_b}) \tag{36}$$

$$S_{2_b} = \frac{\epsilon h_{ba}\rho_{m_b}Gg_{m_b}y'}{\dot{m}_bC_{\mathrm{F}_i}\sigma_{0_b}} \sum_S \frac{C_{S_{mb}}}{M_S} \sum_{v=0}^{v_f} H_v(T_{m_b})k_{Sv}(T_{m_b}) \tag{37}$$

In Eqs. (34-37), $\epsilon = 4.54\times10^4$ J/mole represents the energy difference between vibrational levels for HF, which we have assumed to be constant, G is the geometric parameter, and H_v and F_v are functions of the mixed zone temperature which are defined in Ref. 1. The parameter $a_p(v)$ is the fraction of HF pumped into the vth vibrational level by the pumping reaction, Eq. (19), and σ_{0_b} represents the gain cross section for the $v=1$ to 0 transition, given explicitly by Eq. (36) of Ref. 1, evaluated at the mixed zone temperature of the B region.

Equation (33) is similar in form to Eq. (43) of Ref. 1 which is its counterpart for the pure source flow case. Differences arise because the flow in the B region represents only part of the total flow, hence, the $\dot{m}_b/\dot{m}$ term, and because there is an additional term in Eq. (33) to account for the change in η due to entrainment of the source flow.

In deriving Eqs. (36) and (37), we have assumed that the reaction rate for the collisional deactivation by species S,

$$\mathrm{HF}(v) + S \rightarrow \mathrm{HF}(v') + S \tag{38}$$

can be represented by the rate

$$k_S^{v,v'}(T_{m_b}) = k_S^{sq}(T_{m_b})g_{sq}(v) + k_S^{mq}(T_{m_b})g_{mq}(v), \quad v' = v-1$$
$$= k_S^{mq}(T_{m_b})g_{mq}(v) \qquad v' \le v-2 \tag{39}$$

The deactivation parameter k_{Sv} is related to these rates by the equation

$$k_{Sv}(T_{m_b}) = k_S^{sq}(T_{m_b})g_{sq}(v) + \tfrac{1}{2}v(v+1)k_S^{mq}(T_{m_b})q_{mq}(v) \tag{40}$$

The contribution to η from the source flow region is given by

$$\left(\frac{\mathrm{d}\eta}{\mathrm{d}r}\right)_A = \frac{\theta_a}{\theta}\left[\frac{\mathrm{d}}{\mathrm{d}r}(\eta_{\max_a}X_{T_a} - S_{l_a}) - D_aX_{T_a} - S_{2_a}\right] \tag{41}$$

D_a and S_{2_a} are similar to D_b and S_{2_b} except that h_{ba} is replaced by h_a, $\dot{m}_b$ is replaced by $\dot{m}_a = \theta_a \dot{m}/\theta$, the geometric factor G is taken to be unity, and all the b subscripts are replaced by a subscripts to denote that the parameters are evaluated using the mixed zone properties of the A region. To obtain S_{l_a} and $\eta_{\max_a}$ from Eqs. (35) and (36), the subscripts are changed from b to a and, in addition, the two parameters are multiplied by the term $\sin\theta/\theta$. This term arises because in the A region mass flux is evaluated using the arc length $r\theta$ whereas the extent of the lasing zone is evaluated using the semichord $r\sin\theta$. This difference does not arise in the B region where both the mass flux and the extent of the lasing zone are based on the same length h_{ba}.

Equations (33) and (41) complete the lasing analysis. Prior to achieving the threshold condition, specified by Eq. (32), $(d\eta/dr)_A$ and $(d\eta/dr)_B$ are zero and Eqs. (33) and (41) can be solved for the mixed zone gains which appear in the terms S_l and S_2. Once threshold is achieved, three equations are necessary to specify η and the two gains. Two equations are provided by the threshold condition, Eq. (31), and the net lasing efficiency equation, Eq. (28). The third equation is obtained by noting that the total radiation intensity passing through the A and B regions at a given value of r must be identical. Thus, Eqs. (29) and (30) are coupled through the intensity term. Eliminating this term between the two equations leads to the required third equation

$$\left(\frac{d\eta}{dr}\right)_B = \frac{h_{ba} g_{m_b} G}{h_a g_{m_a}} \left(\frac{d\eta}{dr}\right)_A \tag{42}$$

When $d\eta/dr$ becomes zero once again, lasing terminates and Eqs. (33) and (41) are again solved for the gains g_{m_a} and g_{m_b} with $(d\eta/dr)_A = (d\eta/dr)_B = 0$.

The total temperature change in the B region can now be evaluated with the result that

$$\left(\frac{dT_{0_b}}{dr}\right)_R = \frac{C_{F_i}}{c_p M_F}\left[\frac{dX_{T_b}}{dr} - E(X_{T_a} - X_{T_b})\right]$$

$$\times \left[H - \epsilon \sum_{v=0}^{v_f} v a_p(v)\right] + \frac{C_{F_i}}{c_p}(D_b X_{T_b} + S_{2_b}) \tag{43}$$

where the two terms represent the heat addition due to the pumping reaction and collisional deactivation. H in Eq. (43), equal to 1.27×10^5 J/mole, is the heat of reaction for the pumping reaction. The corresponding equation for the A region is obtained by eliminating the entrainment term and changing the b subscripts to a's.

With the specification of the equations for η, the model for the source flow laser is complete. Aside from the various auxiliary relationships, our model consists basically of eight coupled, ordinary differential equations; Eq. (1) for M_a, Eq. (10) for θ_a, Eqs. (3-6) for the gasdynamic properties of the B region, and Eqs. (33) and (41) for the chemical specific efficiency in each region.

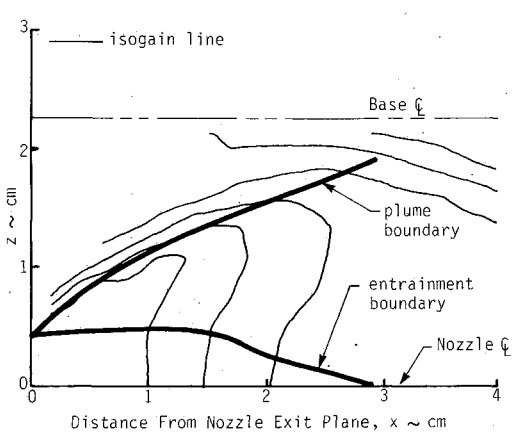

Fig. 3 Gain contours for a source flow nozzle.

D. Base Pressure Correlation

To specify the base pressure for the analysis, we have developed a correlation which appears to work well for a wide range of operating conditions.[4] The correlation is based on the calculation of a critical wake closure base pressure p_{bc} defined as that value of p_b which leads to a final flow pressure, far downstream of the nozzle exit, equal to p_b. It corresponds to the case when the downstream pressure is communicated to the base region either through subsonic boundary layers along shrouds surrounding the laser cavity or through an open wake between nozzles.

For experiments where no particular care is exercised to limit the pressure feedback along the shroud boundary layer, base pressure measurements yield a value equal to p_{bc} to within approximately 10%. For configurations that inhibit pressure feedback, the base pressure can be reduced to approximately 50-70% of p_{bc}. For those configurations, the ratio of p_b to p_{bc} is a useful measure of how successfully the base region has been isolated from the downstream flow.

III. Application of the Model

The primary objective of this section is to use the model we have developed to assess the impact of the base pressure on laser performance. First, however, we will show some comparisons of the model's predictions with experimental results.

Figure 3 shows a plot of the gain contours in a source flow chemical laser, as determined by experiment,[10] for a nozzle with the following characteristics: $r_i = 0.76$ cm, $\theta = 31.8$ deg, $h = 2.3$ cm. For this particular experiment the lasing molecule was DF. Each curve in the figure represents a line of constant gain. The curve crossing the nozzle centerline nearest the nozzle exit plane corresponds to a gain of 0.04 cm^{-1} and each subsequent curve represents a decrement of 0.02 cm^{-1}. The three isogain contours near the base centerline represent absorption with $g = -0.06$ cm^{-1} near the base centerline, -0.04 cm^{-1} for the intermediate curve, and -0.02 cm^{-1} for the curve farthest from the base centerline.

Superimposed on the figure are the entrainment and plume boundaries as predicted by our model with $v_f = 3$ and the kinetic rates appropriate for DF. If the flow within the entrainment boundary were pure source flow, the gain would be constant along each arc of radius $r = r_i + x$. The source flow

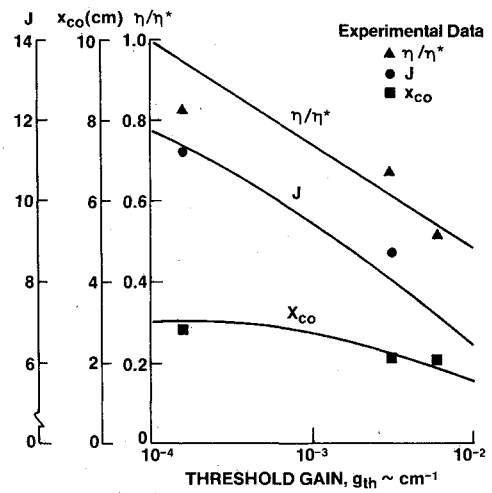

Fig. 4 Comparison of predicted saturation characteristics with experimental data.

Table 1 Baseline conditions

Nozzle geometry:	$r_i = 4.64$ cm, $h = 3.92$ cm, $\theta = 22$ deg
Flow properties:	$M_i = 3.26$, $T_{0_i} = 1130$ K, $\gamma = 1.47$ $\rho_i v_i = 0.502$ g/cm^2-s, $T_{m_i} = 561$ K $C_{F_i}/C_{H_{2i}}/C_{DF_i}/C_{He_i}/C_{N_{2i}}$ $= 0.197/0.104/0.410/0.151/0.139$
Threshold gain:	$g_{th} = 0.0002$ cm^{-1}
Laminar mixing:	$m = 0.5$

assumption for the flow within the entrainment boundary appears justified by the gain contours which are predominantly functions of the distance from the nozzle exit plane. In addition, the entrainment boundary appears to correlate remarkably well with the point where the gains begin to exhibit a much more complex spatial dependence. For this particular experiment the base pressure is approximately 0.42 times the nozzle exit pressure so that the entrainment boundary represents the leading edge of an expansion fan. The figure clearly indicates that the gain in the region between the entrainment and plume boundaries, which is our B region, has an average gain which differs from the source flow gain at the corresponding r. In this case, the gain in the B region is higher because of the lower pressure in the base region. Obviously, our simple one-dimensional model cannot predict the complex spatial variations of the gain which arise partly because entrainment actually occurs gradually through an expansion fan and partly because of the viscous interactions with the recirculating flow in the wake of the plume. Nonetheless, our basic assumption of two distinct flow regions correlates well with the gasdynamics represented by the gain contours. In that regard, it is worth noting that the isogain contours reflect remarkably well many features of the flowfield, including the viscous interactions near the plume boundary and the shock structure at the plume impingement point.

Figure 4 shows a more quantitative comparison with experimental data. Here we have plotted the model's predictions of the effect of threshold gain on lasing performance for a source flow HF laser with the following geometric characteristics: $r_i = 1.27$ cm, $\theta = 31.8$ deg, $h = 3.1$ cm. Shown in the figure are the chemical specific efficiency, the mode length x_{co} which is the distance dowstream from the nozzle exit where lasing cutoff occurs, and the rotational quantum number J which maximizes η for a given value of threshold gain. In plotting η, we have normalized the curves to η^*, the predicted value at $g_{th} = 0.0001$ cm^{-1}. In performing the calculations we assumed $v_f = 2$ and used the reaction rates specified in Ref. 1. Also plotted in the figure are experimental data points taken from Ref. 11. The experimental value of J represents the power-weighted average rotational quantum number for all the lasing lines.

In general, the predicted saturation trends agree well with the experimental data. The model accurately predicts the decrease in the mode width with increasing g_{th}. Because of our assumption that all lasing lines operate at the same J, we would expect some discrepancy between the predicted value of J and the power-weighted average J determined from experiment. Even so, the error in J in Fig. 4 is, at most, less than one. The decrease in η with increasing threshold gain appears to be adequately modeled except for an overprediction by about 12% in the value of η at the lowest gain point. It should be mentioned, however, that it is difficult to accurately establish the threshold gain for cavities with extremely high mirror reflectivities because significant increases in g_{th} above the value predicted by Eq. (32) can result from mirror degradation, or from small amounts of scattered radiation which may go undetected.

We now turn our attention to determining the effect of base pressure on laser performance. For this study we will use the baseline conditions shown in Table 1. As a measure of performance, we will use the chemical specific efficiency ratio, defined as the ratio of η for a specific geometry and base pressure to η_{SF}, the specific efficiency obtained for the same geometry based on a pure source flow calculation.

In Fig. 5 we have plotted this ratio for the baseline conditions in Table 1 as a function of the base pressure ratio p_b/p_{bc} for mixing lengths of 4 and 12 cm. For these conditions $p_{bc} = 6.23$ Torr, which is greater than the nozzle exit pressure of 5.48 Torr. For both values of l_m, η increases as the base pressure decreases, primarily because collisional deactivation in the base region decreases with decreasing p_b. For the lower value of l_m, however, the increase in η is not very large because most of the lasing energy is extracted before a significant fraction of the source flow is entrained into the base region. As the mixing length is increased, lasing cut-off occurs farther downstream, and η is more sensitive to the value of the base pressure, as evidenced by the $l_m = 12$ cm curve which varies from $\eta/\eta_{SF} = 0.87$ at $p_b = p_{bc}$ to $\eta/\eta_{SF} = 1.02$ at $p_b = 0.5\ p_{bc}$. The pure source flow model

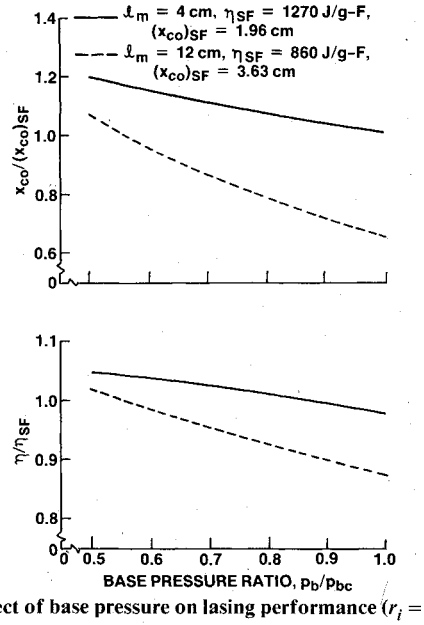

Fig. 5 Effect of base pressure on lasing performance ($r_i = 4.64$ cm).

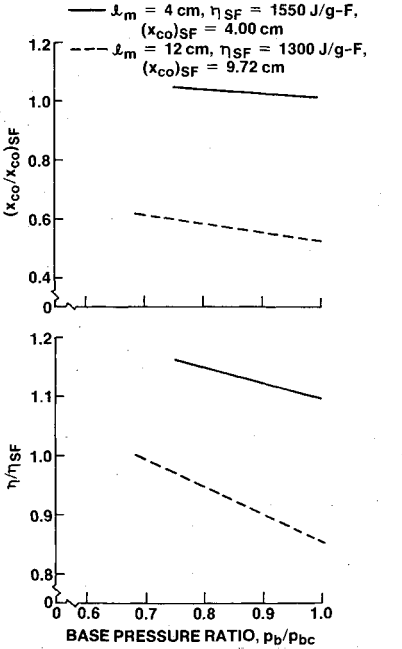

Fig. 6 Effect of base pressure on lasing performance ($r_i = 2.32$ cm).

predicts an increase in η with decreasing l_m, as can be seen by comparing the values of η_{SF}. Figure 5 suggests that this basic conclusion remains unaltered when we compare performance at a given value of p_b. Finally, we note that the lasing efficiency actually can exceed the pure source flow value at the lower values of p_b/p_{bc}, the reason being that the base region becomes a more favorable lasing region when its pressure is lower than the source flow pressure.

Also shown in the figure is the mode length x_{co} normalized to the corresponding value for a pure source flow calculation. (Note the difference in the scale of the ordinate for the x_{co} and η curves.) As expected, lasing terminates sooner for the higher values of p_b. Comparison of the two curves in Fig. 5 shows that the base pressure has a proportionately larger effect on x_{co} than on η. For example, although $\eta = 0.87\eta_{SF}$ for $p_b = p_{bc}$ and $l_m = 12$ cm, the mode length is only 65% of the pure source flow value.

Figure 6 shows another plot of lasing performance with base pressure. The conditions used to generate the curves in this figure are identical to those listed in Table 1 except that the initial source flow radius has been reduced to one-half its baseline value. For the smaller r_i, the curves are not plotted for p_b less than about $0.7p_{bc}$ because for lower values of p_b the model predicts that the outer edge of the plume strikes the base centerline before lasing terminates. Complex gasdynamic interactions occur at the impingement point which are not included in our analysis.

Again, we note that an increase in lasing performance accompanies a decrease in p_b. However, some differences in Figs. 5 and 6 are apparent. At the smaller r_i, η/η_{SF} remains greater than unity even at $p_b = p_{bc}$ for the $l_m = 4$ cm curve. This is because p_{bc}, which equals 2.23 Torr, remains considerably lower than the source flow pressure out to the end of the lasing zone. At the longer mixing lengths, cutoff is delayed sufficiently, so the source flow pressure eventually drops below p_{bc}. Thus, for $l_m = 12$ cm, η/η_{SF} is less than unity for p_b near p_{bc}. Again, for a given value of p_b, we note that a shorter mixing length leads to a higher chemical specific efficiency. Figure 6 shows also that for the smaller radius nozzle the effect on p_b on x_{co} is greater than its effect on η. Comparison of Figs. 5 and 6 shows that another prediction of the pure source flow model, namely, an increase in efficiency with a decrease in r_i, is also unaltered by including the effects of the base region.

IV. Summary and Discussion

In this paper we have developed a simple model for incorporating the effects of base pressure on the performance of source flow chemical lasers. A number of assumptions were introduced either to make the analysis tractable or to describe, at least qualitatively, physical processes that are now only poorly understood. Nonetheless, comparison with small signal gain contours and laser saturation experiments indicates that the model can predict the general gasdynamic characteristics of the flowfield and its lasing properties.

The model has been used in this paper to determine the effect of base pressure on performance. The model predicts that the chemical specific efficiency and the mode length of the laser increase as the base pressure decreases as long as lasing terminates before the plume impinges the base centerline. The gains in η and x_{co} with decreasing p_b occur because of the decrease in collisional deactivition which accompanies a decrease in pressure. The sensitivity of lasing performance to the base pressure is greater for longer mixing lengths and smaller r_i because in both cases the point where lasing terminates occurs farther downstream. Thus, the base region becomes a larger fraction of the lasing volume.

Including base pressure effects causes the chemical specific efficiency to deviate from that predicted by the pure source flow model. The value of η can either be less than or greater than η_{SF} depending on whether p_b is greater than or less than the source flow pressure during the extraction of the lasing energy. For a fixed value of p_b/p_{bc}, however, the results of the current model appear to substantiate the conclusions based on the pure source flow model, namely, that a shorter mixing length and a smaller radius lead to higher efficiencies, provided that plume impingement occurs after lasing cutoff.

In practice, the shortening of the mode at high values of the base pressure may prove more harmful than the decrease in chemical specific efficiency. For example, the shorter mode allows less margin for error in aligning the optical components and, for unstable resonators, limits the capability of reducing the high mirror fluxes. In any case, the deleterious effect of a high base pressure on both η and x_{co} suggests that laser designers either exploit configurations where the base pressure can be maintained at a low value, or else consider features, such as enhanced mixing, which limit the sensitivity of performance to the value of the base pressure.

Acknowledgments

This work was supported in part by the Defense Advanced Research Projects Agency and in part by the Department of the Army. The authors express their appreciation to Mr. Wilford Smith for his assistance in the numerical calculations.

References

[1] Patterson, K. E., Batteh, J. H., and Howie, S. S., "Model for Pure Source Flow Chemical Lasers," *AIAA Journal*, Vol. 21, Feb. 1983, pp. 253-261; see also, AIAA Paper 82-399, Jan. 1982.

[2] Murthy, S. N. B., Ed., *Progress in Astronautics and Aeronautics, Aerodynamics of Base Combustion*, Vol. 40, AIAA, New York, 1976.

[3] Shapiro, A. H., *Compressible Fluid Flow, Vol. 1,* Ronald Press, New York, 1953, p. 231.

[4] Patterson, K. E., Batteh, J. H., and Howie, S. S., "Simple Model for Base Pressure Effects in Source Flow Chemical Lasers," AIAA Paper 82-0400, Jan. 1982.

[5] Liepmann, H. W. and Roshko, A., *Elements of Gasdynamics*, John Wiley and Sons, New York, 1957, Chap. 4.

[6] Alber, I. E. and Lees, L., "Integral Theory for Supersonic Turbulent Base Flows," *AIAA Journal,* Vol. 6, July 1968, pp. 1343-1351.

[7] Mirels, H., "Simplified Model of a Continuous Wave Diffusion-Type Chemical Laser—An Extension," *AIAA Journal,* Vol. 14, July 1976, pp. 930-939.

[8] Broadwell, J. E., "Effects of Mixing Rate on HF Chemical Laser Performance," *Applied Optics*, Vol. 13, April 1974, pp. 962-967.

[9] Emanuel, G. and Whittier, J. S., "Closed Form Solution to Rate Equations for a $F + H_2$ Laser Oscillator," *Applied Optics*, Vol. 11, Sept. 1972, pp. 2047-2056.

[10] Cawthra, J. K., Rocketdyne Division of North American Rockwell, private communication, 1981.

[11] Forman, L. S., Rocketdyne Division of North American Rockwell, private communication, 1981.